A novel approach for predicting battery state of charge and health using an Elman Neural Network combined with Particle Swarm Optimization: Validation with Experimental Data from Electrified Vehicles

Matheus Henrique Rodrigues Miranda
Integrated Systems Laboratory, School of Mechanical Engineering – Universidade Estadual de Campinas - UNICAMP, Brazil

Fabrício Leonardo Silva
Institute of Science and Technology of Sorocaba - São Paulo State University - UNESP, Sorocaba, Brazil

Miguel Campino
IN+, Center for Innovation, Technology and Policy Research, Instituto Superior Técnico, Lisboa, Portugal

Gonçalo O. Duarte
Mechanical Engineering Department – Instituto Superior de Engenharia de Lisboa (ISEL), Lisboa, Portugal
IN+, Center for Innovation, Technology and Policy Research, Instituto Superior Técnico, Lisboa, Portugal

Tiago L. Farias
IDMEC – Instituto Superior Técnico, Universidade de Lisboa, Lisboa, Portugal

Ludmila Corrêa de Alkmin e Silva
Integrated Systems Laboratory, School of Mechanical Engineering – Universidade Estadual de Campinas - UNICAMP, Brazil

ABSTRACT

In the context of electromobility, the energy storage system is essential for vehicle autonomy. It represents a significant cost and adds weight, making it one of the most important components of the vehicle. Efficient battery management involves challenges such as optimization, sizing, management strategies, useful life and appropriate disposal. To ensure its safe and efficient performance, a battery management system (BMS) is essential. For this, accurate estimation of the state of charge (SoC) and state of health (SoH) is of major relevance. This paper presents and discusses an approach based on artificial neural networks for estimating the SoC and SoH of lithium-ion batteries in electrified vehicles. The methodology developed uses an Elman-type neural network trained by a multi-objective optimization algorithm based on the particle swarm (MOPSO) for just one battery cell. However, an algorithm is also presented that associates this neural network, trained with a single battery cell in different series and parallel arrangements, to describe different battery topologies. The accuracy of this methodology was validated using a set of experimental data obtained from a real-world driving cycle performed by duly instrumented electrified vehicles.

INTRODUCTION

Advances in research related to decarbonizing the vehicle fleet have driven the development of new technologies and approaches, such as the use of alternative fuels [1,2] and the creation of new technologies to power electric machines [3], in the case of electrified vehicles. In Brazil, electrification, together with the use of ethanol, has been the main focus of the automotive sector [4], while in Europe, due to the energy matrix, various studies have been carried out on the impact of electric vehicles and the use of hydrogen as an energy source [5]. However, the solution that has emerged and been consolidated in various scenarios is using electrified vehicles, whether purely electric or hybrid electric. Most of these vehicles use lithium-ion batteries, which are responsible for storing and supplying electricity to the motors, impacting both the range and the operating cost of these vehicles [6]. Several developments have occurred, such as advances in chemistry and thermal management [7], as well as battery management systems (BMS).

Batteries are complex and non-linear components due to internal processes during charging and discharging. These processes cause variations in the internal temperature of the components, which, in turn, affect the internal resistance of

each cell. These factors make it necessary to implement a system for monitoring, estimating, and managing battery characteristics, i.e. a BMS. The BMS is implemented to ensure operational safety and increase battery lifespan [8,9]. As such, the BMS performs various functions, most notably estimating the state of charge (SoC) and state of health (SoH), which are fundamental parameters for correct energy management. However, estimating these parameters becomes complicated due to the complex physics of batteries, which depend on internal and external characteristics of their operation, such as temperature and current consumption [10]. Traditional SoC and SoH estimation approaches, based on specific models or calibration methods, may not be robust enough to deal with variations in battery configurations, such as different architectures, temperature action, or charging and discharging profiles, resulting in inaccurate estimates. Thus, various approaches have been applied to predicting the SoC and SoH of batteries, such as the Kalman filter, the particle filter, fuzzy control, support vector machines, artificial neural networks, and combinations of these methods [11, 12, 13].

These approaches are generally used to predict SoC or SoH, with few studies integrating the prediction of these two characteristics simultaneously. Several studies focus on SoH, since with the growth in sales of electrified vehicles, it is essential to monitor and predict battery lifespan. In addition, the process of determining the useful life of a lithium-ion battery is very costly and time-consuming, as it takes around 4.5 hours to complete and requires approximately 1000 cycles for an accurate estimate, which implies around 6 months of experimental testing [14]. Thus, the application of these approaches also aims to reduce the need for multiple cycling tests on these batteries.

In this context, the application of machine learning methods, more specifically artificial neural networks, has proved to be efficient, using different approaches and architectures [15, 16, 17]. Nevertheless, the need for a vast database that includes different battery topologies, voltages, and capacities makes it impossible to adapt the method, often limiting it to the battery configurations present in the database.

To propose a solution that allows the method to be generalized to different battery topologies, Miranda et al. [18] propose a holistic approach in their work, which aims to predict the SoC and SoH of lithium-ion batteries. The methodology developed combines the Elman framework neural network (ENN) with the multi-objective particle swarm optimization algorithm (MOPSO). This neural network framework is known for its ability to deal efficiently with time series data and highly non-linear processes [19]. The method is based on training the ENN using MOPSO, where all the characteristics of the network can be adjusted in an attempt to find the architecture that best adapts to the problem. To achieve the universatility of their method, the researchers trained their algorithm using data from a single battery cell. They then developed an algorithm that associates this cell's neural network with different series and parallel arrangements. This approach allows for the simulation of various battery setups. In the paper, the researchers also presented a series of comparisons with other methods and validations; however, due to the scarcity of real data, no validation was carried out with data from vehicles in real-world operating conditions.

Therefore, this study aims to validate the methodology proposed by Miranda et al [18], using experimental data from different electrified vehicles in real-world driving cycles. For this validation, two plug-in hybrid electric vehicles and one electric vehicle were instrumented, and the required data was collected during operation under real-world conditions. The batteries of these vehicles were then assembled using the algorithm developed by Miranda et al. [18], and the real on-road operating profile was applied. As a result, a curve representing the variation of the SoC over time was obtained, which was then compared with the SoC curve obtained experimentally. This comparison aims to consolidate the accuracy and effectiveness of the proposed methodology, validating its applicability in various operating scenarios.

THEORETICAL ELECTRICAL MODEL OF THE BATTERY

Lithium-ion batteries stand out as the leading choice for electrified vehicles due to their advantages, such as high energy density, long service life, low self-discharge rate and rapid recharging capacity [20]. These batteries are made up of individual cells, which contain a graphite anode, a metal oxide cathode and an electrolyte, which can be liquid or solid. Electrical energy is stored during the charging process by transferring lithium ions from the anode to the cathode. The cells can be connected in series or parallel to achieve different voltages and capacities.

In this work, a modeling of the battery will be presented to obtain the parameters of the SoC and SoH. There are various methods for estimating these parameters [21], however, the approach used here is based on Shepherd's principle, which offers a general model of the dynamics of rechargeable batteries [22].

The SoC of the battery is a parameter that indicates the remaining capacity. This value is commonly expressed as a percentage, with 100% being the maximum charge of the battery and 0% being the total depletion of the charge. Equation (1) describes the calculation of the SoC based on the initial state of charge (SoC_{init}), the battery's actual capacity (Q_{bat} [Ah]) and the current consumed (I_{bat} [A]). In contrast to the SoC, there is also the Depth of Discharge (DoD) of the battery, as represented in Eq. (2).

$$SoC(t) = SoC_{init} - \left(\frac{1}{Q_{bat}(3600)} \int_0^t I_{bat}(t)\, dt\right) \times 100 \qquad (1)$$

$$DoD(t) = 100 - SoC(t) \qquad (2)$$

The battery's dynamic voltage V_{bat} [V] is determined by Eqs. (3) and (4) [22, 23]. The low-frequency electric current I^* [A] values are positive during the charging process and negative during discharging, corresponding to the battery recharge and discharge models, respectively.

$$V_{bat}^{(I^*<0)} = E_0 - RI_{bat} - K\left(\frac{Q_{bat}}{I_{bat}t - 0.1Q_{bat}}\right)I^* - K\left(\frac{Q_{bat}}{Q_{bat} - I_{bat}t}\right)I_{bat}t + Ae^{(-BI_{bat}t)} \quad (3)$$

$$V_{bat}^{(I^*>0)} = E_0 - RI_{bat} - K\left(\frac{Q_{bat}}{Q_{bat} - I_{bat}t}\right)I^* - K\left(\frac{Q_{bat}}{Q_{bat} - I_{bat}t}\right)I_{bat}t + Ae^{(-BI_{bat}t)} \quad (4)$$

where E_0 [V] is the constant voltage of the battery's equivalent circuit, R [Ω] is the internal resistance, I_{bat} [A] is the battery's electric current, K [V/Ah] is the polarization constant, A [V] is the amplitude of the exponential zone, and B [1/Ah] is the exponential zone time constant inverse.

Battery degradation is the decrease in a battery's capacity over repeated charge and discharge cycles. One of the most common models for describing battery aging was proposed by Motapon et al [24]. This model stands out for its generalist approach, which does not require battery cycling experiments, making it a widely used tool for estimates. However, it is important to highlight that the equations used do not consider the thermal effect of the battery cells.

Thus, the SoH is based on the battery's performance throughout its lifetime. A complete cycle is the process in which the battery is fully discharged (SoC = 0%) and then recharged to its maximum capacity (SoC = 100%). Each battery has a maximum number of cycles it can undergo. However, under real-world conditions, a complete cycle, where the battery is fully discharged and then recharged to its maximum, rarely occurs. For this reason, battery life is typically evaluated based on the number of equivalent cycles.

Each discharge and charge cycle impacts the battery's capacity, resulting in its degradation. For the k_{th} equivalent cycle, the battery degradation index ϵ can be determined as a function of the DoD and the cycle number constant (H). This degradation index is described by Eq. (5). The maximum number of cycles until the end of the battery's useful life, denoted as C_l, can be calculated by Eq. (6). The average electric current during the equivalent cycle is denoted by I_{aC} [A] with a stress factor of γ_C for the battery charge and by I_{aD} [A] with a stress factor of γ_D for the discharge process.

$$\epsilon(k) = \epsilon(k-1) + \frac{0.5}{C_l(k-1)}\left(2 - \frac{DoD(k-2) + DoD(k)}{DoD(k-1)}\right) \quad (5)$$

$$C_l(k) = H\left(\frac{DoD(k)}{100}\right)^{-\xi} e^{-\Psi\left(\frac{1}{T_{ref}} - \frac{1}{T_{amb}^{(k)}}\right)} \left(I_c^a(k)\right)^{-\gamma c}\left(I_d^a(k)\right)^{-\gamma d} \quad (6)$$

where the stress factor due to battery discharge is represented by ξ, the Arrhenius constant is indicated by ψ, the reference ambient temperature is given by T_{ref} [K], and the ambient temperature by T_{amb} [K].

By determining the degradation index ϵ, it is possible to calculate the battery's capacities at the beginning (Q_{BOL} [Ah]) and at the end of its useful life (Q_{EOL} [Ah]). Thus, battery degradation can be determined using Eq. (7), which considers the aging factor ϵ over the k_{th} half cycle, where a complete cycle is defined as the process of discharging and recharging the battery.

$$Q(k) = Q_{BOL} - \epsilon(k)(Q_{BOL} - Q_{EOL}) \quad (7)$$

In turn, the increase in the internal resistance of the equivalent circuit R, is determined in the same way, as shown in Eq. (8).

$$R(k) = R_{BOL} + \epsilon(k)(R_{BOL} - R_{EOL}) \quad (8)$$

Therefore, the battery's SoH is a parameter that allows to assess its degradation. It is determined by the ratio between the battery's current capacity Q_k and its capacity at the start of its useful life Q_{BOL}, as shown in Eq. (9). According to the ISO 12405-2 standard [25], the battery reaches the end of its useful life when its discharge capacity reaches 80% of its initial capacity (SoH = 80%).

$$SoH(k) = \frac{Q_k}{Q_{BOL}} \quad (9)$$

DEVELOPED APPROACH

This section discusses the methodology proposed in a previous work by Miranda et al. [18] for predicting SoC and SoH. The approach uses the neural network type called Elman, which is composed of input layers, hidden layers, and output layers. However, the difference between ENN and other frameworks is the presence of a context layer. This layer stores data and sends state information, with each neuron in the context layer interacting with the neurons in the hidden layer. This feature contributes to the ENN making more accurate predictions.

The basic operation of ENN consists of the neurons in the layers receiving signals, processing the information, and sending a response signal to the next layer. Each input signal

to the neuron is multiplied by a corresponding weight, which reflects the relative importance of that input in the neuron's decision-making. This means that inputs with higher weights have a more significant influence on the neuron's output. In addition, the weighted signals are added to a bias value, which allows for an adjustment or activation level, even when the weighted sum is zero.

After the weighted sum and the addition of the bias, the resulting value is submitted to an activation function. This function determines the neuron's response based on the weighted sum, thus deciding whether the neuron will send a signal.

To enable an adaptive training process, where the best ENN architecture is defined, the researchers implemented the neural network in Matlab/Simulink®. The aim of this approach is to allow all the characteristics of the network to be determined during the training process. This includes defining the number of hidden layers, the number of neurons in each layer (hidden and context layer), the weights and biases that influence the connections between neurons, as well as the type of activation function used in each neuron, and the associated parameters. Voltage [V], capacity [Ah], and current [A] are used as inputs.

Miranda et al. [18] emphasize that this flexibility in the choice of network architecture can lead to improved performance, compared to the use of a rigid and fixed architecture, where only the weights and biases are optimized, as occurs in some existing software. This approach reduces processing time and computational cost, making it possible to evaluate and identify the ideal neural network structure without the need to carry out several training sessions.

To ensure that the training process achieves the best combinations of ENN parameters for predicting SoC and SoH, the authors used the heuristic MOPSO algorithm. Four criteria were defined for training: minimizing the root mean square error (RMSE) between the experimental SoC values and the values estimated by the network, minimizing the RMSE of the SoC derivative over time, minimizing the RMSE between the experimental and estimated SoH values and, finally, minimizing the RMSE of the SoH derivative over time. Additionally, an equation correlating the maximum and minimum values of the Pareto frontier is utilized to identify the configuration that offers the best trade-off among all four criteria.

With the aim of developing a network capable of adapting to different battery topologies, Miranda et al. [18] used a series of tests carried out on a Panasonic 18650PF lithium-ion cell, according to the data provided by Kollmeyer [26]. This data reflects the cell's behavior under various operating conditions. The choice to carry out the training with a single cell aims to ensure the generality of the method, allowing different battery configurations to be simulated in series and parallel.

In this context, Miranda et al. [18] also propose an algorithm capable of identifying and assembling battery packs according to voltage and capacity requirements using the ENN trained with data from a single cell. However, as the individual behavior of each cell directly impacts the performance of the battery, balancing the cells is essential to equalize their capacities and ensure that all cells contribute in a balanced way to the operation of the battery pack. To this purpose, the modeling considers the use of an active balancing control, which offers advantages in terms of precision and efficiency in the distribution of energy between the cells in the pack. Thus, equations are presented for cases in which the cells are connected in series, as well as when these series cell modules are interconnected in parallel, achieving an algorithm that assembles the battery pack.

The network's input data consists of the battery's voltage [V], current [A], and capacity [Ah]. The network's expected results are the battery's SoC and SoH, considering the operating conditions represented by the input values. Figure 1 illustrates the framework of the neural network used, where N_n indicates the number of neurons in the layer determined by the training process.

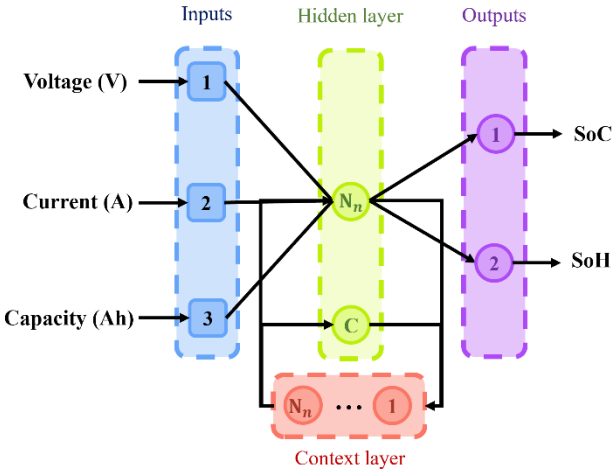

Figure 1. ENN framework used. Adapted from Miranda et al. [18].

This model was evaluated under constant current and voltage conditions, as well as under dynamic discharge conditions. However, none of these validations considered real-world vehicle operating conditions. Therefore, the current work aims to utilize and validate the ENN obtained, together with the battery pack assembly algorithm. It is crucial to highlight that only the existing methodology is applied, and no new training has been conducted. As there is limited data, from the point of view of determining the SoH, only the results for the SoC will be covered. To do this, experimental data from real-world driving cycles of different electrified vehicles will be used.

EXPERIMENTAL ON- ROAD DATA

In order to collect data and evaluate the methodology proposed by Miranda et al. [18], instrumentation and data acquisition were carried out on three electrified vehicles: two plug-in hybrid electric vehicles (PHEVs) and battery electric vehicle (EV). Data was collected during a real-world driving cycle using a variety of experimental equipment. The equipment used included an on-board diagnostic (OBDII) reader to collect information on the operation of the vehicles and a global positioning system (GPS) with a barometric altimeter, Garmin GPSMap76CSx, which provided data on the topography of the road, such as speed, route, and altimetry. In the case of PHEV, a portable emissions measurement system (PEMS) was also used (MET 6.3, MAHA).

This equipment provides a detailed characterization of the trip, collecting data at 1 Hz. The information covers driving dynamics (speed, acceleration), information from the internal combustion engine in PHEVs (such as air mass, engine rotations per minute and load, throttle position, among others), the state of charge of the vehicle battery, the torque of the electric motors and the battery temperature (in the case of EV), as well as the altimetry of the road, which was monitored using information captured by the barometric altimeter [27].

To integrate all the information, the devices were connected to a laptop computer running LabVIEW software, which enables synchronized data collection on a second-by-second basis. The layout of the devices in the vehicle is shown in Fig. 2.

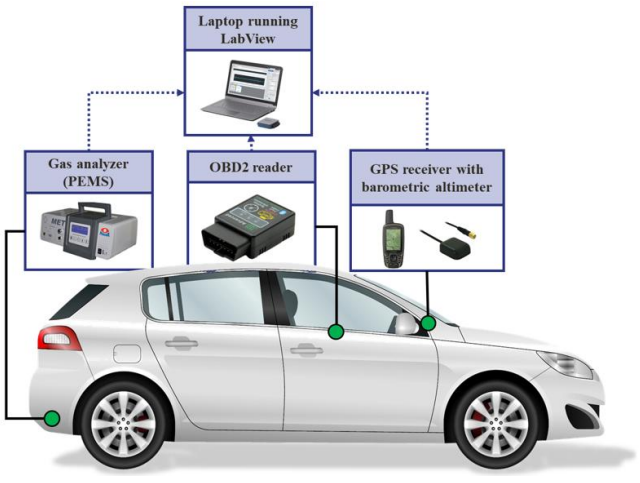

Figure 2. Schematic of the acquisition system.

The tests were carried out on vehicles with batteries of different configurations. One of the PHEVs, vehicle A, belongs to the SUV (Sport Utility Vehicle) category, while vehicle B is a sedan. Vehicle C is an EV in the SUV category, which has a range of 416 km, indicating that its battery has greater capacity than the PHEVs. The characteristics of the batteries in each of these vehicles are shown in Table 1.

Table 1. Vehicles battery specifications.

	Vehicle A	**Vehicle B**	**Vehicle C**
Nominal voltage	293 V	352 V	400 V
Nominal capacity	10 kWh	8.8 kWh	50 kWh

The data was obtained under real-world driving cycles. The route was fixed, and each vehicle was subjected to two trips. The route took place in the metropolitan area of Lisbon, Portugal. It began with an urban section, followed by a section of highway, and then returned to the urban section. The total duration of the trip was approximately two hours, resulting in approximately 7,000 seconds of data collected. The route taken is shown in Fig. 3. The tests were carried out in the morning and afternoon to avoid being influenced by temperature and traffic conditions.

Figure 3. The real driving cycle path.

Furthermore, due to the distinct characteristics of each vehicle, energy management varies considerably between models. Each vehicle adopts its control systems and strategies, which have a direct impact on energy consumption. As a result, the SoC at the end of the trip shows different values for each vehicle model. This not only reflects the capacity of the battery but also these particularities of energy management. Table 2 presents the initial and final SoC for each vehicle during the trips.

Table 2. Initial and final SoC of vehicles for each trip.

	Vehicle A	Vehicle B	Vehicle C
First trip	100% - 2%	81.5% - 13.3%	76% - 59.9%
Second trip	99% - 4%	82.7% - 13.7%	93.7% - 78%

METHODOLOGY

The current consumed is fundamental information used in the model. In the case of EVs, this information is obtained directly from OBDII. However, in PHEVs, this information is unavailable on the OBD reader. Furthermore, for safety reasons, it is not recommended to insert a sensor directly into the circuit to measure the current consumption. This makes it necessary to use alternative methods to estimate the electrical energy consumed.

There are some indirect methods to estimate electrical energy consumption. In this work, the approach based on the variation in battery energy will be adopted, following the methodology described by SAE J1711 [28]. The standard specifies that energy is calculated by subtracting the final current from the initial current and multiplying the result by the system voltage. However, since the current is not measured directly, the solution is to use the variation in SoC values to estimate this current.

The current can be calculated using Eq. (10), where I represent the current in amperes (A), P is the power consumed in watts (W), and V is the battery voltage in volts (V).

$$I = \frac{P}{V} \tag{10}$$

Thus, the power consumed in the PHEV can be estimated based on the variation in battery energy [28]. Equation (11) describes the energy (E) stored in the battery as a function of capacity (C [Ah]) and voltage (V [V]).

$$E = C \times V \tag{11}$$

Therefore, the variation in battery energy, i.e., the energy consumed (ΔE) over the SoC variation, can be determined according to Eq. (12). To manipulate the units, it is necessary to convert the energy from kWh to Joules. To do this, multiply the current by the conversion factor of 3.6 × 10^6 J/kWh.

$$\Delta E = \Delta SoC \times C \times V \tag{12}$$

Once the energy consumed has been determined, the current can be estimated based on the power divided by the battery voltage, as shown in Eq. (13). Hence, this method is based on the relationship between the variation of the SoC, and as the data obtained from the SoC is collected every second, the time interval (Δt) for calculating the current is also one second.

$$I = \frac{\Delta E}{\Delta t \times V} \tag{13}$$

Considering the characteristics of the PHEV batteries and applying these equations, it is possible to obtain the instantaneous values of the current consumed. Figures 4 and 5 show the current consumption graphs for vehicles A and B, respectively, during the first trip.

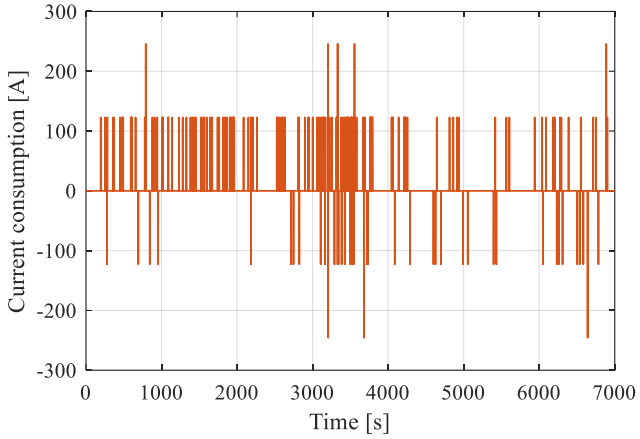

Figure 4. Current consumed by vehicle A on first trip.

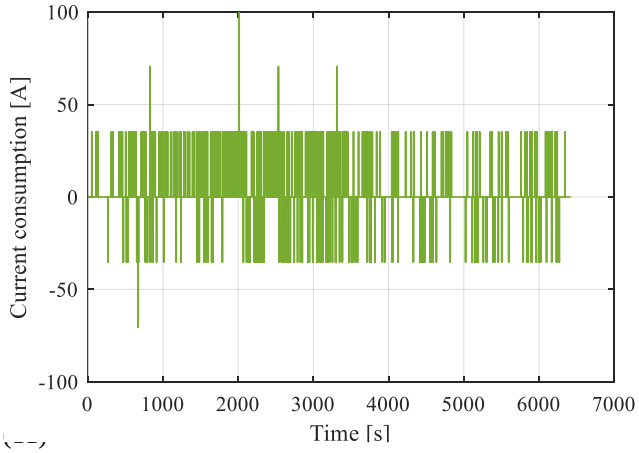

Figure 5. Current consumed by vehicle B on first trip.

In the case of the EV, the current is a variable obtained directly by reading the OBDII port. Figure 6 shows the current values for vehicle C (EV) on its first trip.

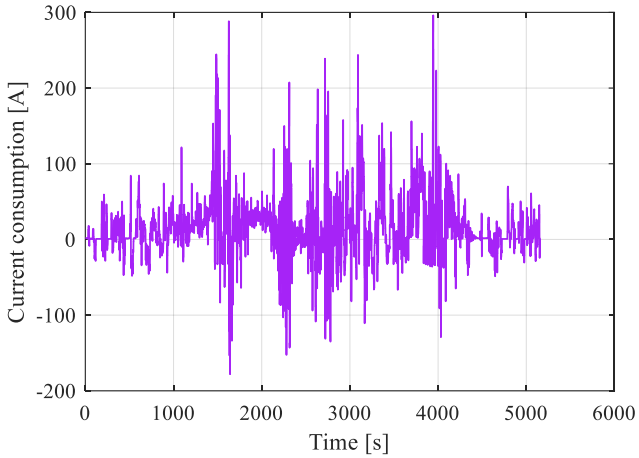

Figure 6. Current consumed by vehicle C on first trip.

After calculating the current of all trips for the three vehicles, the ENN methodology of Miranda et al. [18] can be applied. Three metrics were selected to assess and compare the results of this methodology with experimental values. The first is the Root Mean Square Error (RMSE), which indicates the dispersion between the predicted values and the actual values. Equation (14) describes the RMSE calculation.

$$RMSE = \sqrt{\frac{1}{n}\sum_{i=0}^{t}\left(SoC_{ENN} - SoC_{exp}\right)^2} \quad (14)$$

The second metric used is the correlation coefficient, which assesses the quality of the estimated curve in comparison to the actual SoC curve. This coefficient is calculated based on the sum of the squares of the prediction errors between the values obtained by the methodology and the true values, as shown in Eq. (15). The coefficient ranges from 0 to 1, where 1 indicates a perfect fit between the values, while 0 indicates no correlation between the curves.

$$R^2 = \sqrt{\frac{\left(\sum(SoC_{ENN} - \overline{SoC_{ENN}})\left(SoC_{exp} - \overline{SoC_{exp}}\right)\right)^2}{\sum(SoC_{ENN} - \overline{SoC_{ENN}})^2 \sum\left(SoC_{exp} - \overline{SoC_{exp}}\right)^2}} \quad (15)$$

Moreover, the relative RMSE is also used to provide an additional perspective in the analysis. This metric expresses this error in relative terms, i.e., concerning the actual values. The relative RMSE formula is described in Eq. (16).

$$RMSE_{rel} = \frac{RMSE}{\overline{SoC_{exp}}} \times 100 \quad (16)$$

Therefore, this metric expresses the error as a percentage of the actual average value, which makes it easier to interpret the methodology's performance.

RESULTS

With the necessary data obtained and the evaluation metrics defined, it was possible to assemble the battery pack for each vehicle and evaluate the results. Using the nominal voltage values and battery capacities of each vehicle, the algorithm determines the topology of the pack and the neural network corresponding to the cell is associated with these characteristics.

The battery of vehicle A was assembled by the algorithm, and the current consumed on a second-by-second basis is used in the model. The discharge profile of the experiment (Reference) and that obtained by the model (ENN) for the first trip are shown in Fig. 7. It can be seen that, around the 2500th second, the curves begin to show a slight divergence, but this does not compromise the accuracy of the prediction, as the profile of the curves remains similar. The RMSE between the curves is 1.3302, with a correlation index of 0.9993. In addition, the final SoC value in the experiment was 3%, while the value predicted by the model was 2.82%.

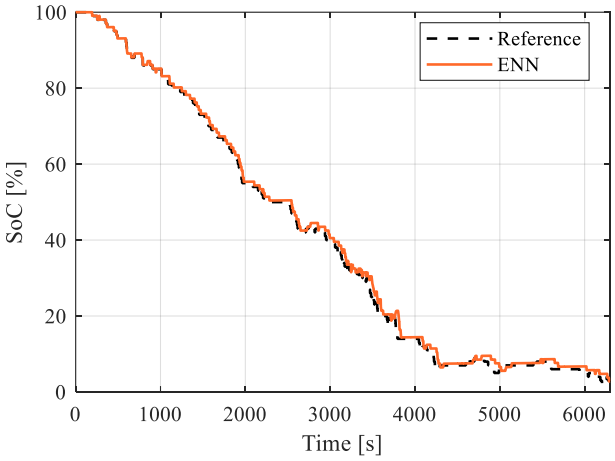

Figure 7. SoC profile of the battery in vehicle A on the first trip.

Figure 8 shows the SoC discharge profile for the second trip of vehicle A. The curves of the experimental values and those predicted by the model perfectly overlap, resulting in a correlation index of 1 and an RMSE of 0.1448.

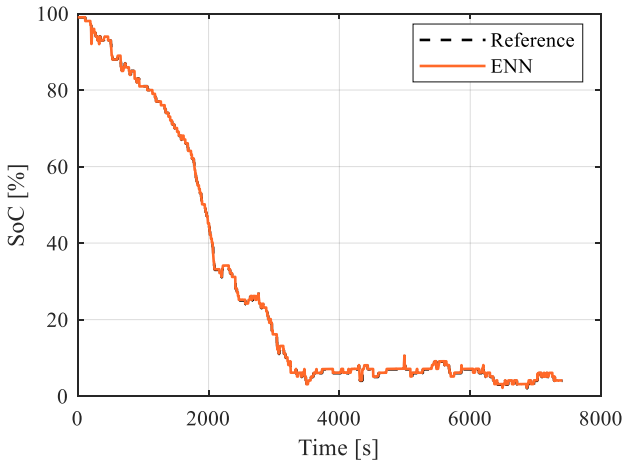

Figure 8. SoC profile of the battery in vehicle A on the second trip.

Table 3 shows the results of the three metrics for the two trips of vehicle A. The relative RMSE for the first trip indicates that the model's error is only 3.3% concerning the average of the reference values. For the second trip, the relative RMSE is even lower, at just 0.5%, showing the accuracy of the methodology.

Table 3. Results of the evaluation metrics for vehicle A.

	First trip	**Second trip**
RMSE	1.3302	0.1448
R^2	0.9993	1.0000
$RMSE_{rel}$	3.2958%	0.5003%

For vehicle B, the same procedure was followed, informing the algorithm of the battery's characteristics for assembling the virtual battery pack. Figure 9 illustrates the discharge profile of the experiment and the model. It is possible to see that, in the case of this vehicle, when the SoC is below 15%, there is a slight discrepancy between the curves. This occurs because when the SoC reaches this level, the system enters charge sustaining mode, which reduces the current flow in the battery to prevent complete discharge. Despite this difference, the correlation index for this trip is 0.99997, with an RMSE of 0.8852. The experimental value of the SoC at the end of the trip was 13.3%, while the value predicted by the model was 14.5%.

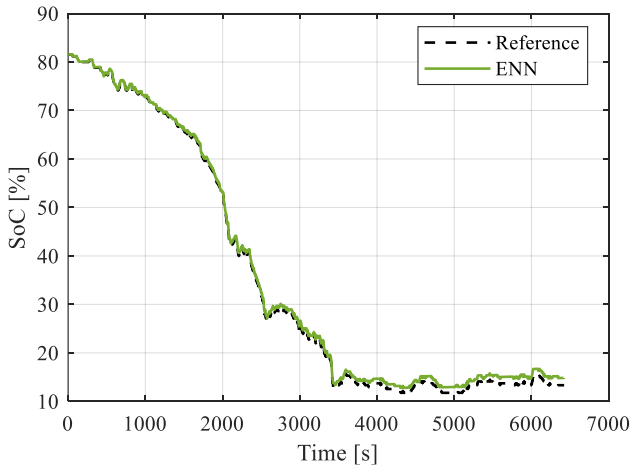

Figure 9. SoC profile of the battery in vehicle B on the first trip.

The SoC profile for the second trip is illustrated in Fig. 10. For this trip, the final SoC values were 13.7% (experimental) and 14.9% (predicted by the model), with an RMSE of 0.8544 and a correlation of 0.99998.

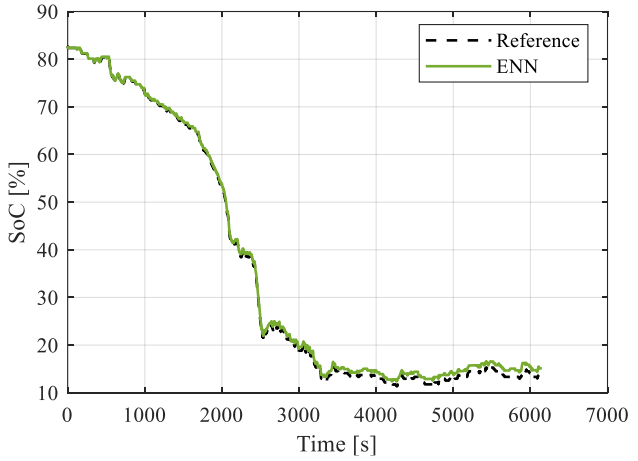

Figure 10. SoC profile of the battery in vehicle B on the second trip.

The error and correlation values for both trips of this vehicle are shown in Tab. 4. Unlike vehicle A, in which a difference was observed between the values of the two trips, vehicle B showed very consistent results for the two conditions analyzed. The relative RMSE for vehicle B was around 2.5%.

Table 4. Results of the evaluation metrics for vehicle B.

	First trip	**Second trip**
RMSE	0.8852	0.8544
R^2	0.99997	0.99998
$RMSE_{rel}$	2.5148%	2.4049%

In the case of the EV (vehicle C), the same methodology was applied, resulting in the assembly of the virtual battery. This vehicle's first trip lasted approximately 5000 seconds, with an initial SoC of 76%. Figure 11 illustrates the behavior of the SoC over this period. The model showed excellent accuracy, with the curves almost completely overlapping. The correlation index of the curves is 1, and the RMSE is 0.0564.

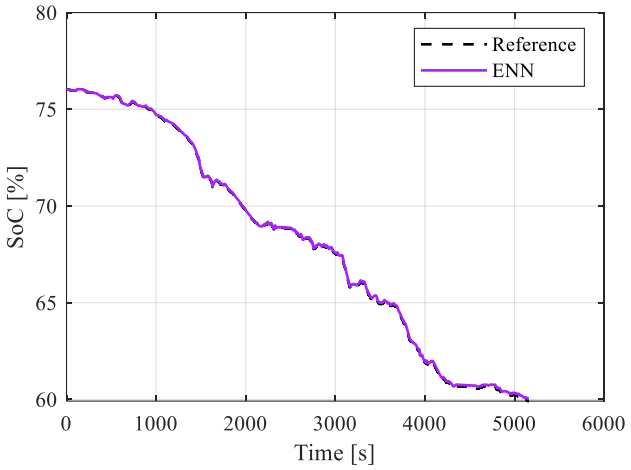

Figure 11. SoC profile of the battery in vehicle C on the first trip.

Figure 12 presents the behavior of the SoC for the second trip. The model again obtained a correlation of 1, with an RMSE of 0.1524.

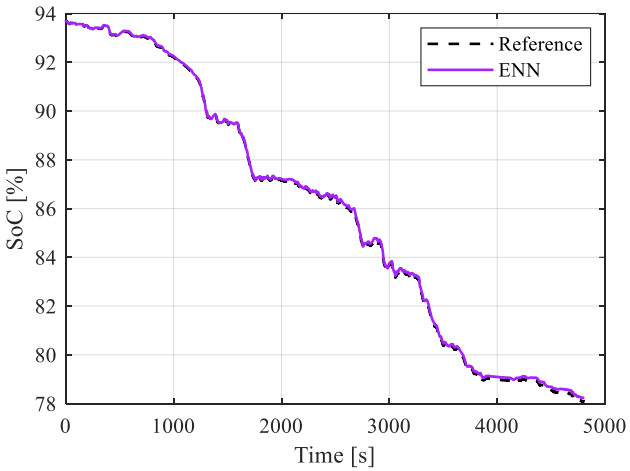

Figure 12. SoC profile of the battery in vehicle C on the second trip.

Table 5 presents the error values for both trips of this vehicle. The relative RMSE for both trips was less than 0.18%, around the average of reference values. This demonstrates the high accuracy of the prediction concerning the experiment.

Table 5. Results of the evaluation metrics for vehicle C.

	First trip	**Second trip**
RMSE	0.0564	0.1524
R^2	1.0000	1.0000
$RMSE_{rel}$	0.1372%	0.1774%

Therefore, the results obtained demonstrate the high accuracy of the model in determining the SoC under real-world operating conditions, regardless of the different topologies and characteristics of the analyzed batteries. It is worth noting that the slight discrepancies observed in the results of the PHEVs (vehicles A and B) may be related to approximations of the current. Additionally, these discrepancies may also be from the rate at which the SoC value is updated by the vehicle's electronic control unit via the OBD port. However, despite these subtle variations, the highest relative RMSE value was only 3.3%, which validates the robustness and accuracy of the proposed methodology.

CONCLUSION

The methodology for predicting SoC and SoH, utilizing the Elman neural network combined with the MOPSO algorithm as proposed by Miranda et al. [18], was evaluated using real-world experimental data.

A dataset was collected containing real on-road operating data from three electrified vehicles: two PHEVs and one EV. The vehicles were properly instrumented to collect the necessary information for evaluating the methodology. The battery pack of each vehicle was assembled virtually. The results indicated that the model closely matched the real SoC values collected, demonstrating its effectiveness.

In this way, the integration of ENN-MOPSO with the battery assembly model, a virtual battery set can be created instantly and easily using the cell's artificial neural network as a basis. This enables real-time prediction of data from any battery topology.

ACKNOWLEDGMENT

This work was conducted with scholarships and financial support from the grant 2024/08117-9, São Paulo Research Foundation (FAPESP), Brazil, the Brazilian National Council for Scientific and Technological Development (CNPq) through grants 308389/2022-0, the Incentive Program for New Professors at Unicamp (PIND) under grants 2500/23, the Universidade Estadual de Campinas - UNICAMP, Brazil, and Instituto Superior Técnico – IST, Portugal. The authors gratefully acknowledge Fundação para a Ciência e Tecnologia (FCT) for funding this research through the following programs: IN+ Strategic

Project (1801P.00962.1.01 - IN+ UIDP/EEA/50009/2025 - IST-ID), grant UI/BD/153621/2022 and financial support via the project LAETA Base Funding (DOI: 10.54499/UIDB/50022/2020). The authors also acknowledge the Project BE.Neutral – Agenda de Mobilidade para a neutralidade carbónica nas cidades, contract number 35, funded by the Resilience and Recovery Plan (PRR) through the European Union under the Next Generation EU.

RERERENCES

[1] BREUER, J.L., SCHOLTEN, J., KOJ, J.C., SCHORN, F., FIEBRANDT, M., SAMSUN, R.C., ALBUS, R., GÖRNER, K., STOLTEN, D. AND PETERS, R. An overview of promising alternative fuels for road, rail, air, and inland waterway transport in Germany. Energies, 15(4), p.1443, 2022.

[2] EL HAFDAOUI, H., JELTI, F., KHALLAAYOUN, A., JAMIL, A. AND OUAZZANI, K. Energy and environmental evaluation of alternative fuel vehicles in Maghreb countries. Innovation and Green Development, 3(1), p.100092, 2024.

[3] HASSAN, Q., AZZAWI, I.D., SAMEEN, A.Z. AND SALMAN, H.M. Hydrogen fuel cell vehicles: opportunities and challenges. Sustainability, 15(15), p.11501, 2023.

[4] GLYNIADAKIS, S. AND BALESTIERI, J.A.P. Brazilian light vehicle fleet decarbonization scenarios for 2050. Energy Policy, 181, p.113682, 2023.

[5] SECK, G.S., HACHE, E., SABATHIER, J., GUEDES, F., REIGSTAD, G.A., STRAUS, J., WOLFGANG, O., OUASSOU, J.A., ASKELAND, M., HJORTH, I. AND SKJELBRED, H.I. Hydrogen and the decarbonization of the energy system in europe in 2050: A detailed model-based analysis. Renewable and Sustainable Energy Reviews, 167, p.112779, 2022.

[6] CAMARGOS, P.H., DOS SANTOS, P.H., DOS SANTOS, I.R., RIBEIRO, G.S. AND CAETANO, R.E. Perspectives on Li-ion battery categories for electric vehicle applications: a review of state of the art. International Journal of Energy Research, 46(13), pp.19258-19268, 2022.

[7] YADLAPALLI, R.T., KOTAPATI, A., KANDIPATI, R. AND KORITALA, C.S. A review on energy efficient technologies for electric vehicle applications. Journal of Energy Storage, 50, p.104212, 2022.

[8] QIU, XIANGHUI; WU, WEIXIONG; WANG, SHUANGFENG. Remaining useful life prediction of lithium-ion battery based on improved cuckoo search particle filter and a novel state of charge estimation method. Journal of Power Sources, v. 450, p. 227700, 2020.

[9] STEINSTRAETER, M., BUBERGER, J., MINNERUP, K., TRIFONOV, D., HORNER, P., WEISS, B., & LIENKAMP, M. Controlling cabin heating to improve range and battery lifetime of electric vehicles. eTransportation, v. 13, p. 100181, 2022.

[10] YANG, R., XIONG, R., HE, H., MU, H., & WANG, C. A novel method on estimating the degradation and state of charge of lithium-ion batteries used for electrical vehicles. Applied Energy, v. 207, p. 336-345, 2017.

[11] XIONG, R., CAO, J., YU, Q., HE, H., & SUN, F. Critical review on the battery state of charge estimation methods for electric vehicles. Ieee Access, v. 6, p. 1832-1843, 2017.

[12] LIU, D., YIN, X., SONG, Y., LIU, W., & PENG, Y. An on-line state of health estimation of lithium-ion battery using unscented particle filter. Ieee Access, v. 6, p. 40990-41001, 2018.

[13] HOW, D. N., HANNAN, M. A., LIPU, M. H., & KER, P. J. State of charge estimation for lithium-ion batteries using model-based and data-driven methods: A review. Ieee Access, v. 7, p. 136116-136136, 2019.

[14] DIAO, WEIPING; SAXENA, SAURABH; PECHT, MICHAEL. Accelerated cycle life testing and capacity degradation modeling of LiCoO2-graphite cells. Journal of Power Sources, v. 435, p. 226830, 2019.

[15] LEE, Jong-Hyun; KIM, Hyun-Sil; LEE, In-Soo. State of charge estimation and state of health diagnostic method using multilayer neural networks. In: 2021 International Conference on Electronics, Information, and Communication (ICEIC). IEEE, 2021. p. 1-4.

[16] DARBAR, Devendrasinh; BHATTACHARYA, Indranil. Application of machine learning in battery: state of charge estimation using feed forward neural network for sodium-ion battery. Electrochem, v. 3, n. 1, p. 42-57, 2022.

[17] HUANG, Z., YANG, F., XU, F., SONG, X., & TSUI, K. L. Convolutional gated recurrent unit–recurrent neural network for state-of-charge estimation of lithium-ion batteries. Ieee Access, v. 7, p. 93139-93149, 2019.

[18] MIRANDA, M. H., SILVA, F. L., LOURENÇO, M. A., ECKERT, J. J., & SILVA, L. C. Particle swarm optimization of Elman neural network applied to battery state of charge and state of health estimation. Energy, v. 285, p. 129503, 2023.

[19] ZHAO, X., XUAN, D., ZHAO, K., & LI, Z. Elman neural network using ant colony optimization algorithm for estimating of state of charge of lithium-ion battery. Journal of Energy Storage, v. 32, p. 101789, 2020.

[20] KOOHI-FAYEGH, S., ROSEN, M. A. A review of energy storage types, applications and recent developments. Journal of Energy Storage, v. 27, p. 101047, 2020.

[21] ZHANG, S., GUO, X., DOU, X., & ZHANG, X. A data-driven coulomb counting method for state of charge calibration and estimation of lithium-ion battery. Sustainable Energy Technologies and Assessments, 40, 100752, 2020.

[22] SHEPHERD, C. M. Design of primary and secondary cells: II. An equation describing battery discharge. Journal of the electrochemical society, v. 112, n. 7, p. 657, 1965.

[23] SAW, L. H., SOMASUNDARAM, K., YE, Y., & TAY, A. A. O. Electro-thermal analysis of Lithium Iron Phosphate battery for electric vehicles. Journal of Power Sources, 249, 231-238, 2014.

[24] MOTAPON, S. N., LACHANCE, E., DESSAINT, L. A., & AL-HADDAD, K. A generic cycle life model for lithium-ion batteries based on fatigue theory and equivalent cycle counting. IEEE Open Journal of the Industrial Electronics Society, 1, 207-217, 2020.

[25] INTERNATIONAL ORGANIZATION FOR STANDARDIZATION (ISO). Electrically propelled road vehicles - test specification for lithium-ion traction battery packs and systems - part 2: High-energy applications. 2012.

[26] KOLLMEYER, P. Panasonic 18650pf li-ion battery data. Mendeley Data, v. 1, n. 2018, 2018.

[27] VARELLA, R. A., FARIA, M. V., MENDOZA-VILLAFUERTE, P., BAPTISTA, P. C., SOUSA, L., & DUARTE, G. O. Assessing the influence of boundary conditions, driving behavior and data analysis methods on real driving CO2 and NOx emissions. Science of the total environment, 658, 879-894, 2019.

[28] SAE – SOCIETY OF AUTOMOTIVE ENGINEERS. J1711 – Recommended Practice for Measuring the Exhaust Emissions and Fuel Economy of Hybrid-Electric Vehicles. Including Plug-in Hybrid Vehicles. SAE International, 2010.